

# Investigating the Properties of Novel Poly(2-hydroxyethyl methacrylate-co-methyl methacrylate) Hydrogel Hollow Fiber Membranes

Ying Luo,<sup>†,§</sup> Paul D. Dalton,<sup>†,§</sup> and Molly S. Shoichet<sup>\*,†,‡,§</sup>

Department of Chemical Engineering and Applied Chemistry, University of Toronto, 200 College Street, Toronto, Ontario, Canada M5S 3E5, Department of Chemistry, University of Toronto, 80 St. George Street, Toronto, Ontario, Canada M5S 1A1, and Institute of Biomaterials and Biomedical Engineering, University of Toronto, 170 College Street, Toronto, Ontario, Canada M5S 3E3

Received April 12, 2001. Revised Manuscript Received September 4, 2001

Poly(2-hydroxyethyl methacrylate-co-methyl methacrylate) hydrogel hollow fiber membranes were synthesized by a novel centrifugal-spinning methodology that resulted in new asymmetric wall morphologies, which in turn affected the mechanical and transport properties. Hollow fiber membranes were formed after polymerizing the comonomers, 2-hydroxyethyl methacrylate and methyl methacrylate, in an aqueous system under centrifugal forces. The concentration of methyl methacrylate in the comonomer and the concentration of redox initiators were investigated for their effects on membrane morphology, water content, Young's modulus, and diffusive transport. Both monomer composition and initiator concentration impacted the resulting asymmetric membrane morphology, which varied from a macroporous sponge to a microporous gel to a homogeneous gel. The hollow fiber membranes synthesized herein had equilibrium water contents between 42 and 57%, elastic moduli between 22 and 400 kPa, and effective diffusion coefficients between  $10^{-7}$  and  $10^{-9}$  cm<sup>2</sup> s<sup>-1</sup> for vitamin B12 and 10 kD dextran. The significant differences in both the moduli and the diffusion coefficients exhibited by these hydrogel membranes reflect differences in their intrinsic microstructures. Synthesis of hydrogel hollow fiber membranes using centrifugal force is a highly dynamic process; the membrane properties can be effectively tailored by controlling phase separation kinetics. These hydrogel hollow fibers are particularly attractive for soft tissue applications, such as nerve guidance channels, where biocompatibility, mechanical strength, and transport properties are determinants of device performance in vivo.

## 1. Introduction

Hollow fiber membranes (HFMs) are used in a diversity of biomedical applications, from bioreactors, to cell encapsulation, to hemodialysis, to nerve guidance channels.<sup>1–4</sup> The choice of material depends on ease of fabrication, low protein adsorption, and overall biocompatibility. HFMs are traditionally produced by extrusion through a spinneret, casting, or dip-coating;<sup>5,6</sup>

HFMs prepared via phase inversion through a spinneret have an asymmetric structure and have been widely used in the separations industry.<sup>7,8</sup> We recently developed a new method to prepare HFMs, “centrifugal spinning”, that is advantageous over other techniques due to its ease and reproducibility.<sup>9</sup> The method is particularly attractive for the synthesis of HFMs of cross-linked networks which are not easily dissolved, a prerequisite for extrusion or dip-coating methods. We are particularly interested in hydrogels because they can be designed to match the mechanical properties of soft tissue, such as nerve, in which we are interested in implanting guidance channels for enhanced nerve regeneration.

Hydrogels have been widely studied for cell encapsulation<sup>10</sup> and drug delivery applications;<sup>11,12</sup> our hydrogel

\* To whom correspondence should be addressed. Tel: 416-978-1460. Fax: 416-978-8605. E-mail: molly@chem-eng.utoronto.ca.

<sup>†</sup> Department of Chemical Engineering and Applied Chemistry, University of Toronto.

<sup>‡</sup> Department of Chemistry, University of Toronto.

<sup>§</sup> Institute of Biomaterials and Biomedical Engineering, University of Toronto.

(1) Nakano, H.; Shinbata, T.; Okumura, R.; Sekiguchi, S.; Fujishiro, M.; Yamane, T. *Biotechnol. Bioeng.* **1999**, *64*, 194–199.

(2) Shoichet, M. S.; Rein, D. H. *Biomaterials* **1996**, *17*, 285–290.

(3) Yamashita, S.; Mochizuki, A.; Nakazaki, T.; Seita, Y.; Sawamoto, J.; Endo, F.; Yui, N.; Ogata, N.; Kataoka, K.; Okano, T.; Sakurai, Y. *ASAIJ* **1996**, *42*, 1019–1026.

(4) Liu, S.; Peulve, P.; Jin, O.; Boisset, N.; Tiollier, J.; Said, G.; Tadie, M. *J. Neurosci. Res.* **1997**, *49*, 425–432.

(5) Ismail, A. F.; Dunkin, I. R.; Gallivan, S. L.; Shilton, S. J. *Polymer* **1999**, *40*, 6499–6506.

(6) Dendunnen W. F. A.; Vanderlei, B.; Robinson, P. H.; Holwerda, A.; Pennings, A. J.; Schakenraad, J. M. *J. Biomed. Mater. Res.* **1995**, *29*, 757–766.

(7) Stern, S. A. *J. Membr. Sci.* **1994**, *94*, 1–65.

(8) Chung, T. S.; Shieh, J. J.; Lau, W. W. Y.; Srinivasan, M. P.; Paul, D. R. *J. Membr. Sci.* **1999**, *152*, 211–225.

(9) Dalton, P. D.; Shoichet, M. S. *Biomaterials* **2001**, *22*, 2661–2669.

(10) Uludag, B.; Roberts, T.; Kharlip, L.; Horvath, V.; Sefton, M. V. *J. Controlled Release* **1993**, *24*, 3–11.

(11) van DijkWolthuis, W. N. E.; Hoogbeem, J. A. M.; van Steenberg, M. J.; Tsang, S. K. Y.; Hennink, W. E. *Macromolecules* **1997**, *30*, 4639–4645.

HFMs may also serve as the vehicles to deliver therapeutic agents in situ. By taking advantage of the asymmetric membrane that is formed during centrifugal spinning, drug release may be manipulated to be either preferentially inward or outward, as has been described in another system to deliver proteins to arterial tissue.<sup>13</sup> We recently reported the use of the centrifugal-spinning technique to create poly(2-hydroxyethyl methacrylate) (PHEMA) hydrogel HFMs.<sup>9</sup> HFMs were prepared by polymerizing HEMA in excess water and under centrifugal forces. Since HEMA is water soluble but PHEMA is water insoluble, as the propagating PHEMA chain grows, it phase-separates out of solution. These phase-separated particles are pushed by centrifugal forces to the periphery of the cylindrical mold in which polymerization is occurring. This process resulted in the formation of concentric PHEMA hydrogel tubes or HFMs. We found that both formulation chemistry (i.e., monomer, initiator, and cross-linking agent concentrations) and rotational speed (or applied centrifugal forces) impacted the geometry of the resulting structure. For tubes to form, phase separation had to occur prior to gelation, otherwise rods resulted.

The PHEMA hydrogel HFMs that we synthesized demonstrated the utility of our centrifugal-spinning technique. These PHEMA HFMs generally had a sponge-like morphology in their wall structure and, consequently, were weak with low elastic moduli (<100 kPa). We believed that the hydrophilic nature of HEMA led to the PHEMA phase separating at the later stages of polymerization, forming elastic particles, and thereby resulting in a loose macroporous morphology. We hypothesize here that addition of a hydrophobic monomer, such as methyl methacrylate (MMA), will enhance phase separation over gelation and thereby facilitate the formation of tubes with higher moduli. Given the highly dynamic process of polymerization–phase separation under centrifugal forces, we anticipate that the polymerization rate will impact the properties of the resulting tubes. Thus, two variables are independently varied—MMA concentration and initiator concentration—and their impact on the resulting structure and properties is examined.

We report herein that by controlling these two formulation parameters (i.e., MMA and initiator concentrations) in the HEMA–MMA centrifugal-spinning system, a variety of novel composite morphological structures and correlated membrane properties arise. By forming a continuous gel-like phase in the membrane, these porous HFMs can withstand the implantation and retrieval procedures required for entubulation strategies in spinal cord and peripheral sciatic nerve injury repair, eliminating the necessity of incorporating additional materials within the tube for mechanical integrity.<sup>14,15</sup> Compared to other materials utilized to fabricate nerve guidance channels,<sup>16,17</sup> the hydrophilic rubbery PHEMA–MMA hydrogel HFMs better mimic the soft tissue into

**Table 1. Formulations Used for PHEMA–MMA HFMs**

fiber code	(HEMA + MMA)/ (water + HEMA + MMA) (wt %)	MMA/ (HEMA + MMA) (wt %)	APS/SMBS (wt % of monomer)	EDMA (wt % of monomer)
M-20	20:80	0	0.5/0.4	0.1
M-25-3	25:75	3	0.5/0.4	0.1
M-25-6	25:75	6	0.5/0.4	0.1
M-25-10	25:75	10	0.5/0.4	0.1
I-0.4	30:70	10	0.4/0.3	0.1
I-0.5	30:70	10	0.5/0.4	0.1
I-0.6	30:70	10	0.6/0.5	0.1
I-0.7	30:70	10	0.7/0.6	0.1

which they are implanted. For example, the Young's modulus of spinal cord tissue was reported to be ~200 kPa,<sup>18,19</sup> which is easily achieved with PHEMA–MMA HFMs. The porous PHEMA–MMA hydrogel allows solute transport and can be permselective. Although there is no conclusive definition of the optimal diffusivity and sieving properties that an artificial tissue membrane should have, semipermeable HFMs have been shown to be advantageous over nonpermeable HFMs in facilitating nerve regeneration.<sup>20,21</sup>

## 2. Experimental Section

**2.1. Materials.** All chemicals were purchased from Aldrich (Milwaukee, WI) and used as received unless otherwise indicated. Vitamin B12 (99%) and fluorescein isothiocyanate–dextran (referred to as dextran and  $M_n$  of 9500 g mol<sup>-1</sup>) were purchased from Sigma (St. Louis, MO). Phosphate buffer saline tablets (Sigma) were used to prepare pH 7.4 phosphate-buffered solute solutions used in the diffusion studies. Water was distilled and deionized using Millipore Milli-RO 10 Plus and Milli-Q UF Plus (Bedford, MA) at 18 M $\Omega$  resistance. Aqueous solutions of ammonium persulfate (APS) and sodium metabisulfite (SMBS) were used together as redox initiators. Ethylene dimethacrylate (EDMA) was the cross-linking agent used in the hydrogel polymerizations.

**2.2. Synthesis of PHEMA–MMA Hydrogel HFMs.** PHEMA–MMA hydrogel HFMs were prepared by copolymerizing HEMA and MMA in a spinning glass tubular mold (Kimble, Vineland, NJ) having an inner diameter of 2.4 mm, as previously described for HEMA alone.<sup>9</sup> The specific formulations used are described in Table 1. Briefly, HEMA and MMA (1 g total), EDMA, and APS were dissolved in water by sonicating for 5 min. This solution was transparent and monophasic to the unaided eye. SMBS was added to the solution, which was then gently agitated for ~15 s prior to injecting it into a glass tubular mold. The mold was sealed at both ends, mounted horizontally into a drill (Heidolph, Germany), and then spun at 2500 rpm at room temperature for 6 h. There was no evidence of phase separation within the solution prior to spinning.

The effects on HFM properties of two variables were independently studied: MMA concentration (M-series) and initiator concentration (I-series), as summarized in Table 1. For the M-series, the concentrations of water, APS, SMBS, and EDMA were held constant at 75, 0.5, 0.4, and 0.1%, respectively. The total monomer concentration was held constant at 25%, but the amount of MMA varied from 3 to 10% of this 25%. For the I-series, the concentrations of water, EDMA, HEMA, and MMA were held constant at 70, 0.1, 27 and 3%,

(12) Torres-Lugo, M.; Peppas, N. A. *Macromolecules* **1999**, *32*, 6646–6651.

(13) An, Y.; Hubbell, J. A. *J. Controlled Release* **2000**, *64*, 205–215.

(14) Li, R. H.; Barbari, T. A. *J. Membr. Sci.* **1996**, *111*, 115–122.

(15) Burczak, K.; Gamian, E.; Kochman, A. *Biomaterials* **1996**, *17*, 2351–2356.

(16) Guest, J. D.; Rao, A.; Olson, L.; Bunge, M. B.; Bunge, R. P. *Exp. Neurol.* **1997**, *148*, 502–522.

(17) Widmer, M. S.; Gupta, P. K.; Lu, L. C.; Meszlenyi, R. K.; Evans, G. R. D.; Brandt, K.; Savel, T.; Gurlek, A.; Patrick, C. W.; Mikos, A. G. *Biomaterials* **1998**, *19*, 1945–1955.

(18) Chang, G. L.; Hung, T. K.; Feng, W. W. *J. Biomech. Eng.* **1988**, *110*, 115–122.

(19) Tunturi, A. R. *Physiol. Chem. Phys.* **1980**, *12*, 373–378.

(20) Rodriguez, F. J.; Gomez, N.; Perego, G.; Navarro, X. *Biomaterials* **1999**, *20*, 1489–1500.

(21) Uzman, B. G.; Villegas, G. M. *J. Neurosci. Res.* **1983**, *9*, 325–338.

respectively. The concentrations of initiators, APS/SMBS, varied from 0.7/0.6 to 0.4/0.3. A homopolymeric PHEMA HFM (with 20% monomer) was fabricated for comparison.

**2.3. Morphology.** The wall morphology of hydrated HFMs was examined with both an optical microscope (Leica MZ-6) and an environmental scanning electron microscope (ESEM, model E-2020, Electroscan Corp., USA). For the latter, an accelerating voltage of 20 kV was used in conjunction with a large spot size and magnifications less than 1500 $\times$ , to limit both heating effects and sample damage. A working distance of 5–7 mm was employed to minimize the scattering of the beam. In the specimen chamber, the pressure was maintained between 500 and 600 Pa and the temperature was maintained at  $1 \pm 0.5$  °C using a Peltier-cooled sample stage. The sample chamber was periodically flushed with water vapor to maintain a satisfactory partial pressure of water, ensuring hydration of the hydrogel. Representative images of the wall morphology are reported.

**2.4. Water Content.** A 0.5 cm HFM segment was equilibrated in water for 48 h, blotted dry, and weighed on a microbalance (Sartorius PT2100, Sartorius Corporation, NY), thereby providing the wet mass. The HFM was then dried under vacuum for 48 h and weighed again, thereby providing the dry mass. The equilibrium water content of the sample was calculated based on the wet mass and the dry mass of the HFM sample according to eq 1. The average and standard deviations of five samples are reported.

$$\text{equilibrium water content\%} = \frac{(\text{wet mass} - \text{dry mass})}{\text{wet mass}} \times 100\% \quad (1)$$

**2.5. Mechanical Testing.** The elastic (or Young's) modulus of the hydrated HFMs was measured using a micromechanical tester (Dynac Dalta, Scientific Instruments, USA). Fiber samples (~3 cm in length) were held at each end with custom-built Luer-Lok grips and pulled apart at a rate of 0.5% min<sup>-1</sup> for 15 s. The tensile force ( $F$ (g)) and the elongation of the HFM were recorded, and the deformation ( $D$ ) was calculated. The inner and outer diameters of the HFM were measured under the optical microscope, and the cross-sectional area ( $S$  (mm<sup>2</sup>)) was calculated. The stress ( $P$ ) applied to the HFM was determined by the tensile force divided by the cross-sectional area according to  $P$  (kPa) =  $F \times 9.8 \times 10^{-3} / (10^3 \times S \times 10^{-6})$ . The apparent elastic modulus ( $E$ ) of the sample was obtained from the slope of the linear fit of the stress vs deformation curve,  $E$  (kPa) =  $(P/D \times 100\%)$ .

**2.6. Diffusive Transport.** **2.6.1. Methodology.** Solute diffusion in a hydrogel is very important to drug delivery applications and has been studied by a number of techniques.<sup>22–24</sup> Diffusive transport experiments were performed here to compare the effective solute diffusion coefficient in different HFMs. We chose a transient diffusion method to study the diffusive transport of the HFMs.<sup>25–27</sup> For this model, the solution within the HFM and the HFM itself are considered as a composite rod. By monitoring the diffusion of the solute from the composite rod to a solute-free reservoir, the effective diffusion coefficient of the membrane was determined using an unsteady-state diffusion model to simulate the mass transfer data. We did not choose a pseudo-steady-state model<sup>28,29</sup>

(22) Sahlin, J. J.; Peppas, N. A. *Macromolecules* **1996**, *29*, 7124–7129.

(23) Pilar, J.; Labsky, J.; Marek, A.; Konak, C.; Schlick, S. *Macromolecules* **1999**, *32*, 8230–8233.

(24) Burke, M. D.; Park, J. O.; Srinivasarao, M.; Khan, S. A. *Macromolecules* **2000**, *33*, 7500–7507.

(25) Stevenson, J. *AIChE J.* **1974**, *20*, 461–466.

(26) Stevenson, J.; Deak, M.; Weinberg, M. *AIChE J.* **1975**, *21*, 1192–1199.

(27) Dinh, S.; Stevenson, J. *J. Membr. Sci.* **1982**, *11*, 127–145.

(28) Cruise, G. M.; Scharp, D. S.; Hubbell, J. A. *Biomaterials* **1998**, *19*, 1287–1294.

(29) Dionne, K. E.; Cain, B. M.; Li R. H.; Bell, W. J.; Doherty, E. J.; Rein, D. H.; Lysaght, M. J.; Gentile, F. T. *Biomaterials* **1996**, *17*, 257–266.

to determine the diffusion coefficient because (1) diffusion either across thick membranes or large solutes is time-consuming and (2) it is necessary to consider boundary resistance on both sides of the membrane and the error caused by convective transport through the membrane.

Two solutes, vitamin B12 having a molar mass of 1300 g mol<sup>-1</sup> and dextran having a number average molar mass ( $M_n$ ) of 9500 g mol<sup>-1</sup> (abbreviated as 10 kD dextran), were used to investigate the diffusive transport of PHEMA–MMA hydrogel HFMs. A 2.8 cm long HFM sample was immersed in a phosphate-buffered (PB) solute solution (5 mg mL<sup>-1</sup> of vitamin B12 or 3 mg mL<sup>-1</sup> of 10 kD dextran) for at least 12 h to equilibrate the hollow fiber wall with the solute solution. The HFM ends were fixed to a plastic adaptor, and the lumen was filled with the solute solution. The HFM was sealed at the ends using 5 min epoxy glue and Teflon plugs. Next, the HFM sample was gently agitated in a fresh, solute-free PB solution for 2 s to remove any loosely adsorbed solute prior to immersing the HFM in a stirred, solute-free PB bath (22 mL). At prescribed time points, the HFM was transferred to a fresh bath and the amount of solute that had diffused from the HFM to the previous bath was determined by either UV analysis (Ultraspec 4000, Pharmacia Biotech, U.K.) for vitamin B12 or fluorescence (SPECTRAMax GEMINI, Molecular Devices, CA) for dextran. At the end of the experiment, the HFM was removed from the holder and placed in a fresh PB bath for at least 48 h to determine the amount of solute remaining in the HFM. All permeability experiments were performed at 37 °C in a water bath. The outer and inner radii of hydrated HFMs were measured before and after the permeability experiment using a light microscope (Leica MZ-6).

**2.6.2. Data Analysis.** The unsteady-state diffusion model, developed by Stevenson et al.,<sup>25,26</sup> was used to analyze the data. The amount of solute that had diffused from the HFM into the sampling bath at a given time ( $M_t$ ) and the total amount of solute initially loaded into the sealed HFM ( $M_0$ ) were used to calculate the fraction,  $R$ , of the solute remaining in the HFM at each sampling time point  $\tau$ , as shown in eq 2

$$R(\tau) = 1 - M_t/M_0 \quad (2)$$

where  $\tau$  is dimensionless diffusion time and is calculated according to eq 3 in terms of the real diffusion time ( $t$ ), the diffusion coefficient ( $D_1$ ) of either vitamin B12 or 10 kD dextran in water, and the outer radius of the HFM ( $b$ )

$$\tau = tD_1/b^2 \quad (3)$$

To determine the effective diffusion coefficient ( $D_{\text{eff}}$ ), a parameter,  $\alpha_1$ , was required and was calculated from the slope of the  $\ln(R)$  vs  $\tau$  curve from the linear regression of data for  $\tau \geq 0.35$ , as shown in eq 4

$$\alpha_1^2 = -\text{slope} = -\frac{d \ln(R)}{d\tau} \quad (4)$$

With  $\alpha_1$  and the geometry of the fiber known, the solute  $D_{\text{eff}}$  was derived from eq 5

$$\frac{D_{\text{eff}}}{D_1} = \frac{1}{\phi(\alpha_1, \kappa)} \kappa \alpha_1 \frac{J_1(\kappa \alpha_1)}{J_0(\kappa \alpha_1)} \ln(1/\kappa) \quad (5)$$

where  $\kappa$  is the ratio of the inner radius ( $a$ ) to the outer radius ( $b$ ) of the HFM ( $\kappa = a/b$ ), and  $J_0(\kappa \alpha_1)$  and  $J_1(\kappa \alpha_1)$  are Bessel functions of the first kind;  $\phi(\alpha_1, \kappa)$  is a correction factor between the unsteady-state permeability and the steady-state permeability.<sup>26</sup>

Thus, the effective diffusion coefficient,  $D_{\text{eff}}$ , is the product of the diffusion coefficient of the solute in the membrane and the equilibrium partition coefficient of the solute in the

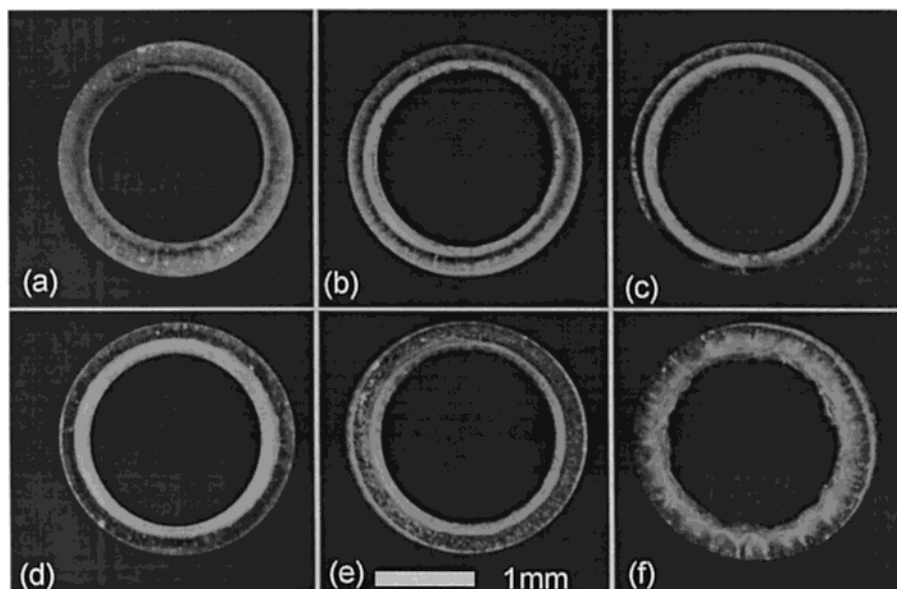


**Figure 1.** Representative light micrographs of hydrogel hollow fiber membrane cross-sections: (a) M-25-3; (b) M-25-6; (c) M-25-10; (d) I-0.4; (e) I-0.5; (f) I-0.7.

membrane and the water. The  $D_{\text{eff}}$  values reported are the average and standard deviations of four HFMs.

### 3. Results

**3.1. Synthesis and Morphology of Hydrogel HFMs.** The properties of HFMs prepared by the centrifugal-spinning technique are determined by the formulation chemistry and the speed of spinning. Under some conditions, rods, instead of tubes, can form.<sup>9</sup> In these studies, we were careful to choose conditions that favored phase separation over gelation for the production of tubes. All tubes had an outer diameter that matched the inner diameter of the mold, i.e., 2.4 mm. For the M-series, the concentration of MMA, with respect to total monomer (HEMA + MMA), varied from 3 to 10% because rods resulted at MMA concentrations less than 3% whereas an immiscible reaction mixture resulted at MMA concentrations greater than 10%. For the I-series, the initiator concentration was varied from 0.4/0.3% to 0.7/0.6% for APS/SMBS because lower initiator concentrations resulted in rods and higher initiator concentrations would not allow sufficient time for the initiated polymerization solution to be transferred to the mold prior to the onset of phase separation.

As shown in Figures 1–3, the wall morphology of the HFMs was influenced by the concentrations of both MMA and initiator. In Figure 1, representative light micrographs demonstrate an overall perspective on the wall morphology of concentric HFMs. All HFMs seem to have a biphasic wall structure, the delineation of which becomes clearer with higher MMA concentrations. As shown in Figure 1c for M-25-10, there appear to be two distinct morphologies, an outer gel phase and an inner sponge phase. Interestingly, the wall thickness decreases with MMA concentration and reaches a plateau value at 6% MMA: wall thickness decreased from  $\sim 320 \mu\text{m}$  for M-25-3 to  $\sim 240 \mu\text{m}$  for M-25-6 and to  $\sim 230 \mu\text{m}$  for M-25-10. This decreased wall thickness may result from compaction of the gel phase during the centrifugal-spinning process.

The change in wall morphology of PHEMA–MMA HFMs with increased MMA concentration is better

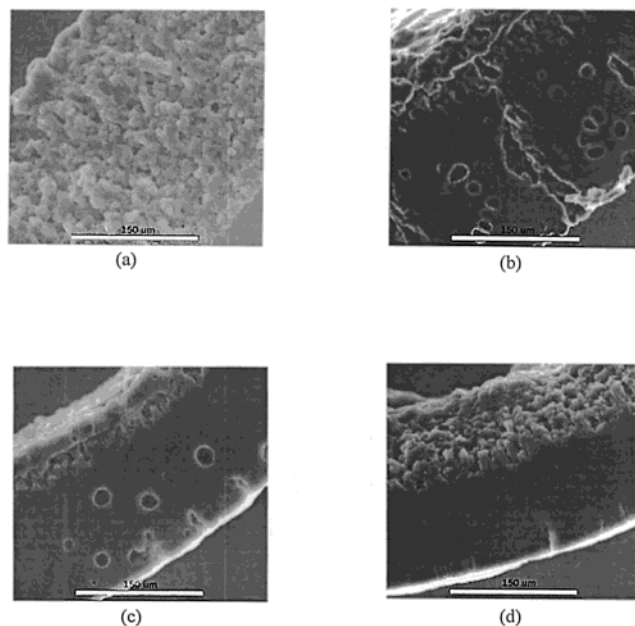


**Figure 2.** ESEM micrographs of the M-series HFMs: (a) M-20; (b) M-25-3; (c) M-25-6; (d) M-25-10.

visualized under the ESEM, as shown in Figure 2. As a point of comparison, a homopolymeric PHEMA HFM (M-20) was examined and observed to have a spongelike structure with bicontinuous polymer and water phases (Figure 2a). The polymer phase consists of a series of connected polymeric droplets and is typical of the heterogeneous structure of PHEMA hydrogels polymerized in excess water.<sup>30</sup> Copolymeric PHEMA–MMA HFMs had a composite structure of sponge and gel. For M-25-3 (Figure 2b), a porous gel morphology resulted with some pores being connected and forming channels across the membrane. For M-25-6 (Figure 2c), a distinct multilayer structure was observed, with a bicontinuous spongelike inner layer and a continuous gel-like outer

(30) Dalton, P. D.; Vijayasekaran, S.; Shoichet, M. S. In *Methods of Tissue Engineering*; Atala, A., Lanza, R., Eds.; Academic Press: San Diego, CA, 2001; Chapter 63, pp 725–731.

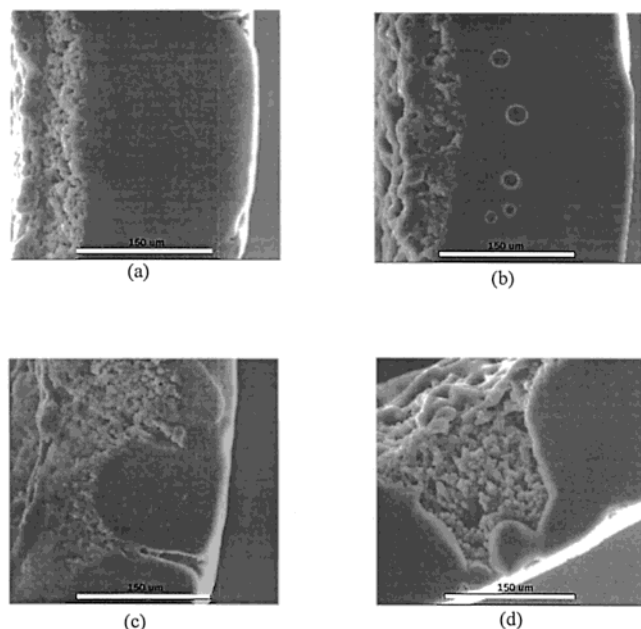


**Figure 3.** ESEM micrographs of the I-series HFMs: (a) I-0.4; (b) I-0.5; (c) I-0.6; (d) I-0.7.

layer throughout which were isolated hydrated pores. At higher MMA concentrations, such as M-25-10 (Figure 2d), two distinct phases were observed: an inner bicontinuous spongelike phase and an outer gel phase with no apparent pores. The gel layer had a morphology similar to homogeneous PHEMA gels<sup>31</sup> and was transparent under the light microscope.

The change in morphology of PHEMA–MMA HFMs with increasing MMA concentration is likely to have resulted from the increased hydrophobicity and decreased solubility of MMA relative to HEMA. Copolymers with higher MMA content are likely to phase-separate out earlier than those with lower MMA content. Furthermore, the decreased swellability of PHEMA–MMA with higher MMA content is reflected in the increased gel phase vs sponge phase.

The concentration of initiator also impacted the resulting wall morphology of the HFMs. All I-series HFMs had a composite morphology of gel and sponge phases as shown in parts d–f of Figure 1 and in Figure 3. In Figure 1, the light micrographs display a general perspective of the wall morphology and concentricity of the HFMs. The ESEM images in Figure 3 provide more detailed information on this morphology. At the lowest initiator concentrations (I-0.4, Figure 3a), where the rate of polymerization was slowest and yet the length of polymer chains was greatest, the HFM had two distinct phases, an inner heterogeneous sponge phase and an outer homogeneous gel phase. The bilayer morphology observed was similar to that of M-25-10 (Figure 2d). The rate of polymerization increased with initiator concentration, resulting in accelerated phase separation and thus an increase in the sponge phase. For I-0.5 (Figure 3b), there was a composite morphology consisting of an inner sponge phase and an outer gel phase, throughout which were dispersed hydrated pores. I-0.5 had a morphology similar to that observed for M-25-6 (Figure

**Table 2. Equilibrium Water Content and Young's Modulus of PHEMA–MMA HFMs**

fiber code	water content (%) $n = 5$	Young's modulus (kPa) $n = 4$
M-20	67.1 ± 6.7	18.0 ± 3.9
M-25-3	54.2 ± 3.0	30.8 ± 7.2
M-25-6	49.6 ± 0.4	45.3 ± 10.3
M-25-10	51.8 ± 2.8	406.7 ± 27.2
I-0.4	43.3 ± 0.8	489.7 ± 37.7
I-0.5	45.8 ± 2.2	253.1 ± 35.8
I-0.6	48.3 ± 1.9	72.2 ± 12.2
I-0.7	50.9 ± 2.1	22.1 ± 1.9

2c). As initiator concentration further increased, the sponge phase also increased. Thus, for I-0.6 (Figure 3c), the sponge phase seemed to overlap with the gel phase and there appeared to be spongelike channels that traversed the wall thickness. This overlapping phase morphology was more pronounced in I-0.7 (Figure 3d) where wider spongelike channels were observed across the wall thickness.

The HFMs were characterized for equilibrium water content, elastic modulus, and diffusive transport. We anticipated a correlation between HFM morphology and these properties.

**3.2. Equilibrium Water Content and Mechanical Properties.** The HFMs were characterized for equilibrium water content by comparing wet and dry masses, as described in eq 1, and for elastic modulus (or Young's modulus), as summarized in Table 2. The highest water content was calculated for M-20 (homopolymeric PHEMA), which had a sponge morphology. Copolymeric PHEMA–MMA HFMs had lower water contents, reflecting the decreased water content of the gel phase relative to the sponge phase. (Homogeneous PHEMA gels have water contents of 40%.<sup>31</sup>) As might be expected, the Young's modulus increased with increased MMA concentration (or increased gel phase), from 18.0 ± 3.9 kPa for M-20 to 30.8 ± 7.2 kPa for M-25-3 to 406.7 ± 27.2 kPa for M-25-10. For the I-series, similar trends were observed: water content increased with initiator concentration (or increased sponge phase). Similarly, Young's modulus decreased with increased initiator concentration (or increased sponge phase). This demonstrates that the strength of the HFMs is dominated by the gel phase and the higher water content is dominated by the sponge phase.

**3.3. Diffusive Transport.** The effective diffusion coefficients of two solutes, vitamin B12 (1.3 kD) and dextran (10 kD) in the HFM, were determined according to eqs 2–5. A typical example of the diffusive transport data analysis is shown in Figure 4. Linear regression was performed for  $\tau \geq 0.35$  to obtain the effective diffusion coefficient, and these results are summarized in Table 3. Both solutes diffused through the M-20 HFM very fast (and indeed before  $\tau$  reached 0.35), making it impossible to calculate the diffusion coefficient. The diffusivity through this sponge membrane is likely to be comparable to that in water as solutes can easily diffuse through the interconnected water phase (or channels).

Given the complex morphology across the HFMs, the effective solute diffusion coefficients are lumped parameters and do not distinguish between diffusion through the gel phase vs that through the sponge phase; however, some imaging techniques may allow local

(31) Peppas, N. A. In *Hydrogels in Medicine and Pharmacy*; Peppas, N. A., Ed.; CRC Press: Boca Raton, 1987; Vol. II, pp 50–62.

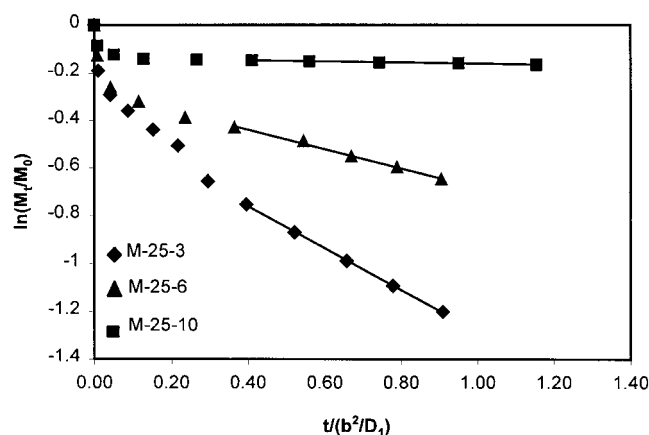


**Figure 4.** Diffusion profile of 10 kD dextran in the M-series HFMs ( $\ln R$  vs  $\tau$ ), and linear regression analysis for HFM diffusion.

**Table 3. Diffusion Coefficients in PHEMA–MMA HFMs ( $n > 3^a$ )**

fiber code	vitamin B12 ( $\times 10^8 \text{ cm}^2 \text{ s}^{-1}$ )	10 kD dextran ( $\times 10^8 \text{ cm}^2 \text{ s}^{-1}$ )
M-20	<i>b</i>	<i>b</i>
M-25-3	$21.3 \pm 3.5$	$8.48 \pm 1.01$
M-25-6	$7.30 \pm 0.81$	$3.43 \pm 1.25$
M-25-10	$0.262 \pm 0.042$	$0.181 \pm 0.014$
I-0.4	$0.160 \pm 0.051$	$0.283 \pm 0.141$
I-0.5	$2.29 \pm 0.61$	$0.531 \pm 0.103$
I-0.6	$11.6 \pm 1.9$	$6.93 \pm 0.51$
I-0.7	$39.9 \pm 1.2$	$13.7 \pm 2.9$

<sup>a</sup> The diffusion coefficients of vitamin B12 and 10 kD dextran in water are  $3.9 \times 10^{-6}$  and  $1.0 \times 10^{-6} \text{ cm}^2 \text{ s}^{-1}$ , respectively.<sup>32–33</sup>

<sup>b</sup> The diffusion was so fast that the diffusive transport could not be simulated.

solute diffusion to be distinguished in a heterogeneous gel.<sup>22–24</sup> The mechanism of solute diffusion was not unique across the HFMs. The solutes are likely to have found the path of least resistance, which would be the interconnected water phase in the sponge structure; across the gel phase, however, solutes had to diffuse through this homogeneous phase, which we anticipated would be most restrictive on diffusive transport. Indeed, as shown in Table 3, diffusive transport decreased with increasing MMA content (for the M-series) for both vitamin B12 and dextran, reflecting the increased gel phase observed by ESEM (Figure 2). Similarly, diffusive transport decreased with decreasing initiator concentration (for the I-series) for both vitamin B12 and dextran, reflecting the increased gel phase observed by ESEM (Figure 3).

The diffusion coefficients of vitamin B12 and dextran in water are  $3.9 \times 10^{-6}$  and  $1.0 \times 10^{-6} \text{ cm}^2 \text{ s}^{-1}$ , respectively.  $D_{\text{eff}}$  in the HFMs for these solutes decreased with increased MMA concentration (i.e., increased gel phase) for vitamin B12 from  $2.13 \pm 0.35 \times 10^{-7}$  for M-25-3 to  $2.62 \pm 0.42 \times 10^{-9} \text{ cm}^2 \text{ s}^{-1}$  for M-25-10, reflecting a decrease of two orders of magnitude. A similar decrease was observed for dextran, from  $8.48 \pm 1.01 \times 10^{-8}$  for M-25-3 to  $1.81 \pm 0.14 \times 10^{-9} \text{ cm}^2 \text{ s}^{-1}$  for M-25-10. Correspondingly, in the I-series,  $D_{\text{eff}}$  decreased with decreased initiator concentration (i.e., increased gel phase). For vitamin B12,  $D_{\text{eff}}$  decreased from  $3.99 \pm 0.12 \times 10^{-7}$  for I-0.7 to  $1.60 \pm 0.51 \times 10^{-9} \text{ cm}^2 \text{ s}^{-1}$  for I-0.4; similarly, for dextran,  $D_{\text{eff}}$  decreased from  $1.37 \pm 0.29 \times 10^{-7}$  for I-0.7 to  $2.83 \pm 1.41 \times 10^{-9}$

$\text{cm}^2 \text{ s}^{-1}$  for I-0.4, reflecting a decrease of two orders of magnitude in diffusion with the change of morphology. Thus, when there was a solid gel layer present in the HFM wall (i.e., M-25-10 and I-0.4), the effective diffusive transport of the solute in the membrane was significantly reduced, with  $D_{\text{eff}}$  being almost two orders of magnitude lower than those of M-25-3 and I-0.7, having a predominantly spongelike structure. The HFMs with hydrated pores in the gel layer (i.e., M-25-6 and I-0.5) exhibited diffusive transport properties between the two extremes.

#### 4. Discussion

The morphologies and properties of HFMs synthesized by the centrifugal-spinning methodology were affected by both MMA concentration, which impacts overall solubility of the propagating chain, and initiator concentration, which impact the overall rate of polymerization. Since MMA is more hydrophobic than HEMA, the PHEMA–MMA propagating radical phase-separates faster than the homopolymeric PHEMA. Phase-separated polymeric particles are denser than water, with PHEMA having a density of  $1.15 \text{ g cm}^{-3}$  and PMMA having a density of  $1.20 \text{ g cm}^{-3}$ ; thus, under the applied centrifugal forces, the polymer-rich phase is pushed to the periphery while the water-rich phase (density of  $\sim 1 \text{ g cm}^{-3}$ ) is pulled to the center. Polymerization is likely to have proceeded in a reduced aqueous environment. This, coupled with the fact that increased MMA concentration resulted in decreased water solubility, favored the formation of the gel phase morphology in the wall and thus decreased equilibrium water content. While we previously found an upper limit for monomer concentration of 20–25% for the formation of homopolymeric PHEMA HFMs (vs rods),<sup>9</sup> this minimum was surpassed by the addition of MMA, which clearly enhances phase separation over gelation.

Although the overall composition of HEMA and MMA in the final polymer is likely to be identical to the monomer feed ratio in this copolymeric system, the local chemical composition is likely to vary across the membrane. Several factors may influence the monomer distribution. We hypothesized above that both density and hydrophobicity of the constituents in the spinning system are critical to HFM morphology and properties. We found this to be true and suggest that the outer HFM wall structure is enriched with MMA. This suggestion is supported by the reactivity ratio data for HEMA and MMA where that monomer with the higher reactivity ratio is incorporated into the polymer at a higher rate and thus is likely to be concentrated in the outer surface of the HFM wall. While the reactivity ratio ( $r$ ) data for HEMA and MMA in water are unknown, in *N,N*-dimethyl formamide,  $r_{\text{HEMA}}$  and  $r_{\text{MMA}}$  are 0.67 and 1.08, respectively.<sup>34</sup> In aqueous media, the reactivity ratio of HEMA is likely to increase due to hydrogen bond interaction. Thus, HEMA and MMA may exhibit similar reactivity toward polymerization. When the centrifugal-spinning method is applied to this copolymeric system,

(32) Boggs, D. R. *Diffusive transport in membranes for immunosolation*; Northwestern University: Evanston, IL, 1994.

(33) Granath, K. A. *J. Colloid Sci.* **1958**, *13*, 308–322.

(34) Mathew-Krotz, J.; Mahadevan, V. *Macromol. Chem. Phys.* **1997**, *198*, 1597–1604.

it is necessary to balance all these controlling factors to manipulate the local chemical composition.

HFM morphology was sensitive to initiator concentration and thus to polymerization rate. At higher initiator concentrations, phase separation increased relative to gelation, resulting in a composite morphology. The morphology (parts c and d of Figure 3) almost implies that PHEMA–MMA phase-separated from the water-rich phase and was then pulled to the periphery by centrifugal forces where gelation was commencing. This contrasts with the morphology observed for lower initiator concentrations where distinct bilayer structures are observed (parts a and b of Figure 3). It is interesting to note that a microporous gel phase morphology resulted from some formulations (i.e., M-25-6 and I-0.5) without the use of porogens. A similar porous morphology was recently reported<sup>35</sup> for PHEMA hydrogels that relied on salt to enhance the phase separation and provided a mechanism for water droplets to be trapped in the gel network during phase separation. In our system, the microporous morphology may result from a HEMA microemulsion as HEMA has been shown to act as a surfactant in a ternary MMA–HEMA–water system.<sup>36</sup> The appropriate conditions during HFM synthesis may have existed for HEMA to have a surfactant effect, which in turn resulted in a gel layer with isolated hydrated pores.

The water content of the HFMs reflected their composite structures, whereas their mechanical and transport properties were dominated by either the sponge or gel phase morphology. For M-25-10, the overall water content of 52% can be rationalized by the composite structure consisting of a homogeneous gel layer with a likely water content of ~40% and a spongy layer with a likely water content of ~67%. For M-25-3, I-0.7, and I-0.6, both mechanical and transport properties reflect the predominantly macroporous (or sponge) wall morphologies. In contrast, for M-25-10 and I-0.4, both

mechanical and transport properties reflect the predominantly homogeneous (or gel) wall morphology. Thus, the gel layer results in solute diffusion resistance and higher Young's moduli. For intermediate morphologies, such as those presented by M-25-6 and I-0.5, where a microporous gel morphology was apparent, the mechanical and transport properties seemed to reflect differences in pore density in their gel layers. The greater diffusive permeability and lower Young's modulus of M-25-6 relative to I-0.5 indicated greater microporosity in the former. Thus, by controlling the wall morphology, the mechanical and the transport properties of the HFM can be precisely tuned.

## 5. Conclusions

PHEMA–MMA hydrogel HFMs were synthesized by a new methodology, centrifugal spinning, that resulted in a diversity of morphologies and mechanical and transport properties. The asymmetric morphology in the HFM wall structure resulted from the highly dynamic phase-separation process. The transport properties were inversely correlated with the mechanical properties, yet each could be tuned to meet the requirements for implantation into soft tissue. The HFM properties were controlled by varying the processing parameters utilized in the centrifugal-spinning technique, which seems to be advantageous over apparently more complicated manufacturing techniques of HFMs. Since centrifugal spinning of hydrogels is aqueous based and in self-contained molds, organic solvents are obviated and the process is clean room compliant. This facilitates scale-up and production of sterile products for implantation. In ongoing studies, we are examining the utility of these tubes for their regenerative capacity in vivo.

**Acknowledgment.** The authors thank Klaus Schultz (Botany, McMaster University) for use of the ESEM. The authors gratefully acknowledge partial financial support from The Whitaker Foundation Biomedical Engineering Research Grant to M.S.S. and a Connaught Scholarship to Y.L.

(35) Liu, Q.; Hedberg, E. L.; Liu, Z.; Bahulekar, R.; Meszlenyi, R.; Mikos, A. *Biomaterials* **2000**, *21*, 2163–2169.

(36) Cheung, H. M. *Langmuir* **1998**, *14*, 757–761.